Electronic Supplementary Material (ESI) for Journal of Materials Chemistry A.

Electronic Supplementary Information

Probing structure-designed Cu–Pd nanospheres and their Pt-monolayer-shell derivatives as high-performance electrocatalysts for alkaline and acidic oxygen reduction reactions

Liuxuan Luo, Cehuang Fu, Shuiyun Shen, Fengjuan Zhu and Junliang Zhang*

Institute of Fuel Cells, Key Laboratory for Power Machinery and Engineering of MOE, School of Mechanical Engineering, Shanghai Jiao Tong University, Shanghai 200240, China.

* E-mail: junliang.zhang@sjtu.edu.cn

CONTENTS:

Experimental section

Chemicals and materials

Palladium(II) acetylacetonate [$Pd(acac)_2$, 99%], copper(II) acetylacetonate [$Cu(acac)_2$, 97%], oleylamine (OAm, 70%), trioctylphosphine (TOP, 90%), copper(II) sulfate ($CuSO_4$, ≥99%), sulfuric acid (H_2SO_4, 95.0∼97.0%), potassium tetrachloroplatinate(II) (K_2PtCl_4, ≥99.9%), acetic acid (>99%), potassium hydroxide (KOH, ≥85%), perchloric acid ($HClO_4$, 70%) and commercial Pd/C (~30%) were all purchased from Sigma-Aldrich. Nafion stock solution (DuPont, 20%), commercial Pt/C (~47%) and carbon black powders (AkzoNobel, EC-300J) were used as received. All of the aqueous solutions in this study were prepared using ultrapure water (Millipore Milli-Q, >18.2 MΩ cm).

Preparation of $^{CG}Cu_1Pd_1$ NSs/C and $^{CG}Cu_1Pd_1$ NSs/C-HT

$^{CG}Cu_1Pd_1$ NSs were synthesized via a facile one-pot solvothermal method based on our previous work.[1] In brief, 13.3 mg of $Pd(acac)_2$ and 40.5 mg of $Cu(acac)_2$ were mixed with 100 μL of TOP and 10 mL of OAm, the mixture was then heated to 240 °C at a constant heating rate under inert atmosphere, and kept for 1 h. After cooling down, the product was washed repeatedly with hexane-ethanol mixtures and then precipitated by a high-speed centrifugation. The as-obtained $^{CG}Cu_1Pd_1$ NSs were finally dispersed in chloroform to form a NSs-chloroform mixture for a further supporting process. In addition, a certain amount of carbon black powders were also mixed with chloroform via sonication to form a well-dispersed carbon-chloroform mixture for the supporting process.

The supporting process was performed via mixing the NSs-chloroform mixture with the carbon-chloroform mixture under continuous stirring, the new mixture was then sonicated for 30 min and further stirred for 12 h. The product was washed repeatedly with ethanol and then precipitated by a high-speed centrifugation. In addition, a thermal-pickling treatment using acetic acid was performed to remove the residual organics on the product.[1–3]

The facile heat treatment was conducted as follows, briefly, the above-obtained $^{CG}Cu_1Pd_1$ NSs/C was placed into a tube furnace and heated to 300 °C at 10 °C min^{-1} under inert atmosphere, and then kept for 1 h before being cooled down. The metal loadings for both $^{CG}Cu_1Pd_1$ NSs/C and $^{CG}Cu_1Pd_1$ NSs/C-HT are ~3.18% for Cu and ~5.00% for Pd.

Formation of Pt MSs

The Pt MSs were generated onto the surfaces of the above-annealed $^{CG}Cu_1Pd_1$ NSs through an electrochemical technology involving Cu UPD and Pt^{2+} galvanic replacement.[2,4–6] Specifically, a certain amount of well-dispersed $^{CG}Cu_1Pd_1$ NSs/C-HT ink was pipetted onto a well-polished glassy carbon electrode (diameter: 5 mm) as the working electrode. The $^{CG}Cu_1Pd_1$ NSs/C-HT ink was prepared by mixing the $^{CG}Cu_1Pd_1$ NSs/C-HT powders with the solution of ethanol and isopropanol, and the mixture was then sonicated for 30 min. After being dried in air, the working electrode was initially placed into a N_2-saturated 50 mM H_2SO_4 solution, and repeated PCs between 0 and 1.10 V were performed at 20 mV s^{-1} to completely eliminate the Cu species on the outermost surfaces of $^{CG}Cu_1Pd_1$ NSs as well as the residual organics. After being thoroughly rinsed using ultrapure water, the working electrode was then placed into an Ar-saturated 50 mM H_2SO_4 and 50 mM $CuSO_4$ solution, in which a steady Cu-UPD CV was obtained at 20 mV s^{-1}. Subsequently, a forward linear potential sweep to 0.90 V was performed to completely remove the UPD Cu atoms on the surfaces of $^{CG}Cu_1Pd_1$ NSs. Then, a backward linear potential sweep to 0.391 V was performed to acquire the Cu MSs on $^{CG}Cu_1Pd_1$ NSs. Immediately, the above-modified working electrode was transferred into an Ar-saturated 50 mM H_2SO_4 and 1.0 mM K_2PtCl_4 solution, and kept for 2 min to completely replace Cu with Pt^{2+}. After being thoroughly rinsed with ultrapure water, the as-prepared working electrode was finally covered with a 3 μL drop of the dilute Nafion solution (0.04%), and dried in air for further electrochemical measurements. The metal loadings for $^{CG}Cu_1Pd_1@Pt_{ML}$ NSs/C-HT are ~3.13% for Cu, ~4.90% for Pd and ~1.72% for Pt.

For all of the electrochemical experiments in this study, a 1 cm^2 Pt foil served as the counter electrode. A saturated calomel electrode coupled with a 1.0 M KNO_3 salt bridge was used as the reference electrode in acidic solutions, while a mercury oxide electrode (Hg/HgO, 1.0 M KOH) coupled with a 1.0 M KOH salt bridge in alkaline solutions. In this study, all of the potentials are referenced to the corresponding reversible hydrogen electrodes (RHEs), and all of the current densities are normalized by the geometric area of the glassy carbon electrode (~0.196 cm^2), unless other mentioned.

Physicochemical characterizations

TEM, high-angle annular dark field–STEM (HAADF–STEM) and HR–TEM images were all acquired on a JEOL JEM-ARM 200F spherical aberration correction transmission electron microscope. STEM–EDS elemental analyses were also obtained via this device with the corresponding detector. It should be noted that nickel grids were used for preparing all of the electron-microscopy samples to avoid the possible interferences to the Cu contents in the samples, which can be induced by the commonly used copper grids. ICP elemental analyses were carried out using a Thermo iCAP7600 ICP–optical emission spectrometer. XRD patterns were recorded on a Bruker D8 ADVANCE Da Vinci poly-functional X-ray diffractometer at 2 deg. min^{-1} with a Cu Kα radiation (λ = 0.15404 nm). XPS analyses were performed on a Shimadzu Kratos AXIS UltraDLD instrument. The raw XPS spectra were calibrated by the C 1s line at 284.80 eV, and then subtracted by backgrounds (Shirley) before deconvolutions.

Electrochemical measurements

All of the electrochemical measurements in this study were carried out using a Metrohm Autolab PGSTAT302N electrochemical workstation in conventional three-electrode cells at room temperature. The working electrodes modified with different electrocatalysts were prepared by the similar procedure in the *Formation of Pt MSs* section. To clean and activate the electrocatalysts,

repeated PCs between 0 and 1.10 V were performed at 100 mV s^{-1} in N_2-saturated 0.1 M $HClO_4$ solutions. Subsequently, steady CVs were obtained at 20 mV s^{-1} in fresh N_2-saturated 0.1 M $HClO_4$ solutions, and the associated forward LSVs were then recorded at 10 mV s^{-1} in O_2-saturated 0.1 M KOH or $HClO_4$ solutions. Electrochemical durability of the electrocatalysts were evaluated by the ADT, via performing the repeated PCs between 0.6 and 1.0 V at 100 mV s^{-1} in N_2-saturated 0.1 M KOH or $HClO_4$ solutions. The associated forward LSVs were recorded after every 10000 and 5000 cycles of the ADT in alkaline and acidic media, respectively.

The ECSA was calculated via the similar methods reported in our previous works.[1,2] In order to be more precise, the charge used in this study is the average value of the adsorption and desorption charges. Besides, the electrocatalytic activity and electron transfer numbers of the electrocatalysts for ORR were also calculated via the same methods detailedly described in our previous work.[2] It is noteworthy that the ORR electrocatalytic activity in this paper are all calculated with both *iR* correction and background calibration. It is also noted that the representative loadings of different electrocatalysts for different electrochemical tests are the respective optimized ones. The representative optimized metal loadings on the electrodes are as follows. (1) For the ECSA evaluations, ~42.89 μg_{Pt} cm^{-2}_{geo} for the commercial Pt/C, ~4.59 μg_{Pd} cm^{-2}_{geo} for $^{CG}Cu_1Pd_1$ NSs/C-HT and ~1.61 μg_{Pt} cm^{-2}_{geo} for $^{CG}Cu_1Pd_1@Pt_{ML}$ NSs/C-HT. (2) For the alkaline ORR electrocatalytic activity evaluations, ~15.31 μg_{Pd} cm^{-2}_{geo} for the commercial Pd/C, ~29.78 μg_{Pt} cm^{-2}_{geo} for the commercial Pt/C, ~2.04 μg_{Pd} cm^{-2}_{geo} for $^{CG}Cu_1Pd_1$ NSs/C and ~2.04 μg_{Pd} cm^{-2}_{geo} for $^{CG}Cu_1Pd_1$ NSs/C-HT. (3) For the acidic ORR electrocatalytic activity evaluations, ~80.06 μg_{Pt} cm^{-2}_{geo} for the commercial Pt/C and ~3.07 μg_{Pt} cm^{-2}_{geo} for $^{CG}Cu_1Pd_1@Pt_{ML}$ NSs/C-HT.

Computational methods

First-principles calculations were carried out based on the DFT through the Vienna *ab initio* Simulation Package.[7–10] All of the models were calculated via the generalized gradient-corrected Perdew-Burke-Ernzerhof functional with the projector augmented wave pseudo-potentials (500 eV energy cut-off).[11,12] A smearing parameter of k_BT = 0.1 eV was used in the Gaussian smearing to accelerate the SCF convergence, and all of the calculations were finally extrapolated to k_BT = 0.

The crystal models were sampled with the 6 × 6 × 6 Monkhorst-Pack grids. After the convergence tests (<1 meV $atom^{-1}$), the 5-layer slabs (pure Pd, pure Pt, CuPd and CuPdPt, Fig. S6), which consisted of the (111) facets, were sampled with the 3 × 3 × 1 Monkhorst-Pack grids in the 2 × 2 × 1 prismatic supercells. The top two layers of the slabs were relaxed while the others were fixed. The dipole correction was used along the *z*-direction. A vacuum of 15 Å was applied to eliminate the interaction between the slabs during the calculation.

The adsorption energy (ΔE_{ads}) of the intermediate on the slab was calculated as follows.[13]

$\Delta E_{ads} = E_{tot} - E_{intermediate} - E_{slab}$

Where E_{tot}, $E_{intermediate}$ and E_{slab} are, respectively, the total energy of the slab adsorbed with the intermediate, the total energy of the dissociative intermediate and the total energy of the bare slab.

The free energy of OH^- (E_{OH^-}) was calculated as follows.[13]

$E_{OH^-} = E_{H_2O(l)} - E_{H^+}$

$E_{H_2O(l)} = G_{H_2O(g)} + RT \times \ln(p/p_0)$

$G_{H^+} = 1/2 G_{H_2} - pH \times kT \times \ln(10)$

(l: liquid; g: gas)

The free energy was calculated as follows.[13]

$G = E + ZPE - TS - neU$

$ZPE = \sum(h\nu_i/2)$

Where *E* is the structure energy, *ZPE* is the zero-point energy, *h* is the Planck constant and ν_i is the vibrational frequency, which are all calculated according to a previous work.[13] *T* is the room temperature (298.15 K), *S* is the entropy, *n* is the number of electrons, *e* is the charge constant and *U* is the overpotential.

The atomic ratios and (111) crystal planes of the four slabs, which represent the associated four electrocatalysts, are all determined based on the XPS-measured surface compositions and the XRD-measured dominant crystal structures proved by the XRD patterns and our previous work.[1] For the CuPd slab representing the annealed $^{CG}Cu_1Pd_1$ NS, all of the atoms in the top two layers of the slab are set as Pd atoms, because the electrocatalyst is first subjected to the activation process in the acidic solution before the ORR electrocatalytic activity testing, in which the Cu species in the outer surface layers of $^{CG}Cu_1Pd_1$ NS can be completely removed. The CuPdPt slab representing $^{CG}Cu_1Pd_1@Pt_{ML}$ NS is constructed by replacing the top layer of Pd atoms in the CuPd slab with Pt atoms, to represent the Pt monolayer shell.

Fig. S1–S8

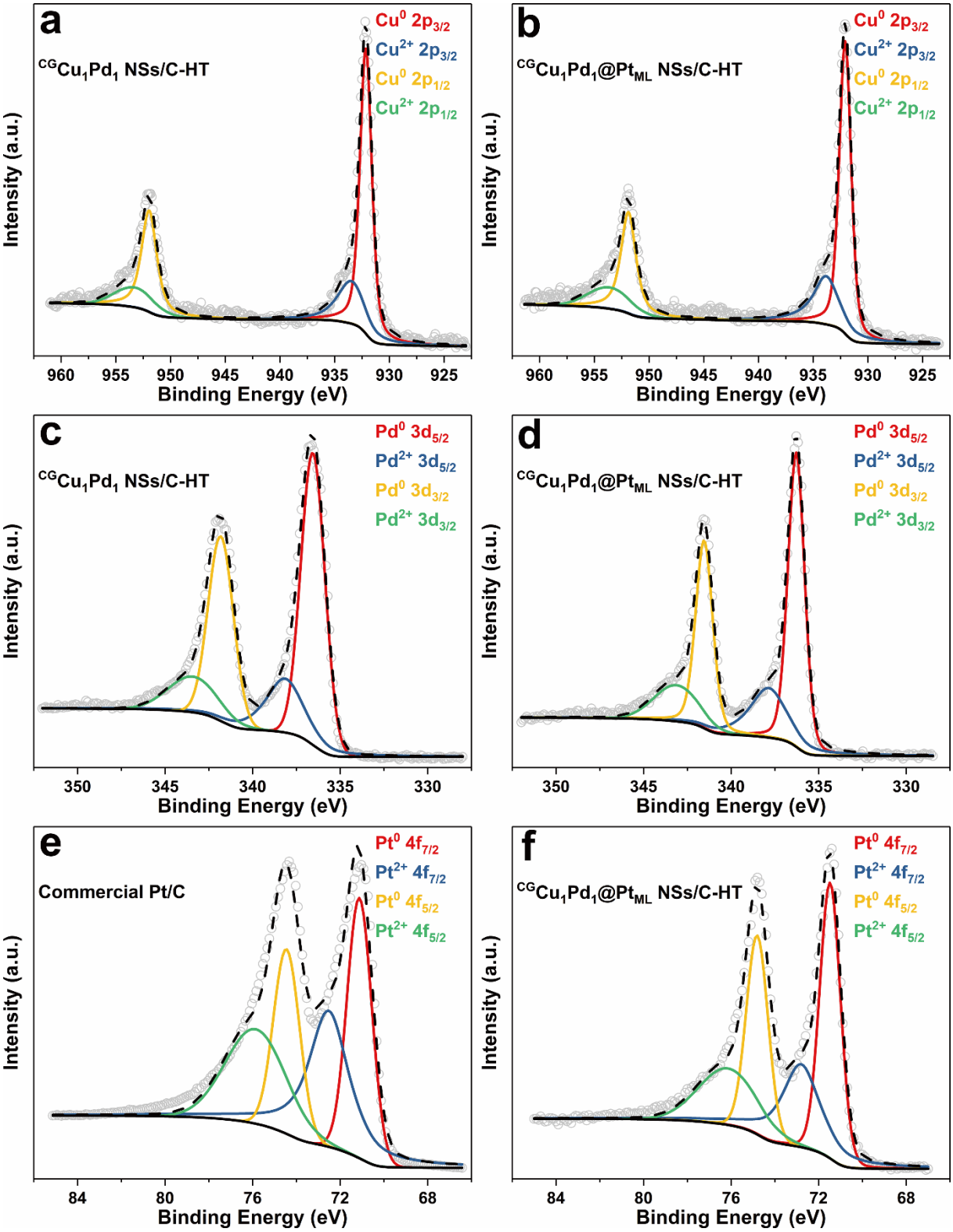

Fig. S1 Representative XPS spectra of the (a and b) Cu 2p, (c and d) Pd 3d and (e and f) Pt 4f for the commercial Pt/C, $^{CG}Cu_1Pd_1$ and $^{CG}Cu_1Pd_1@Pt_{ML}$ NSs/C-HTs. The light-gray circles represent the experimental data, while the black dash lines for the whole fitting results and the black solid lines for the backgrounds (Shirley).

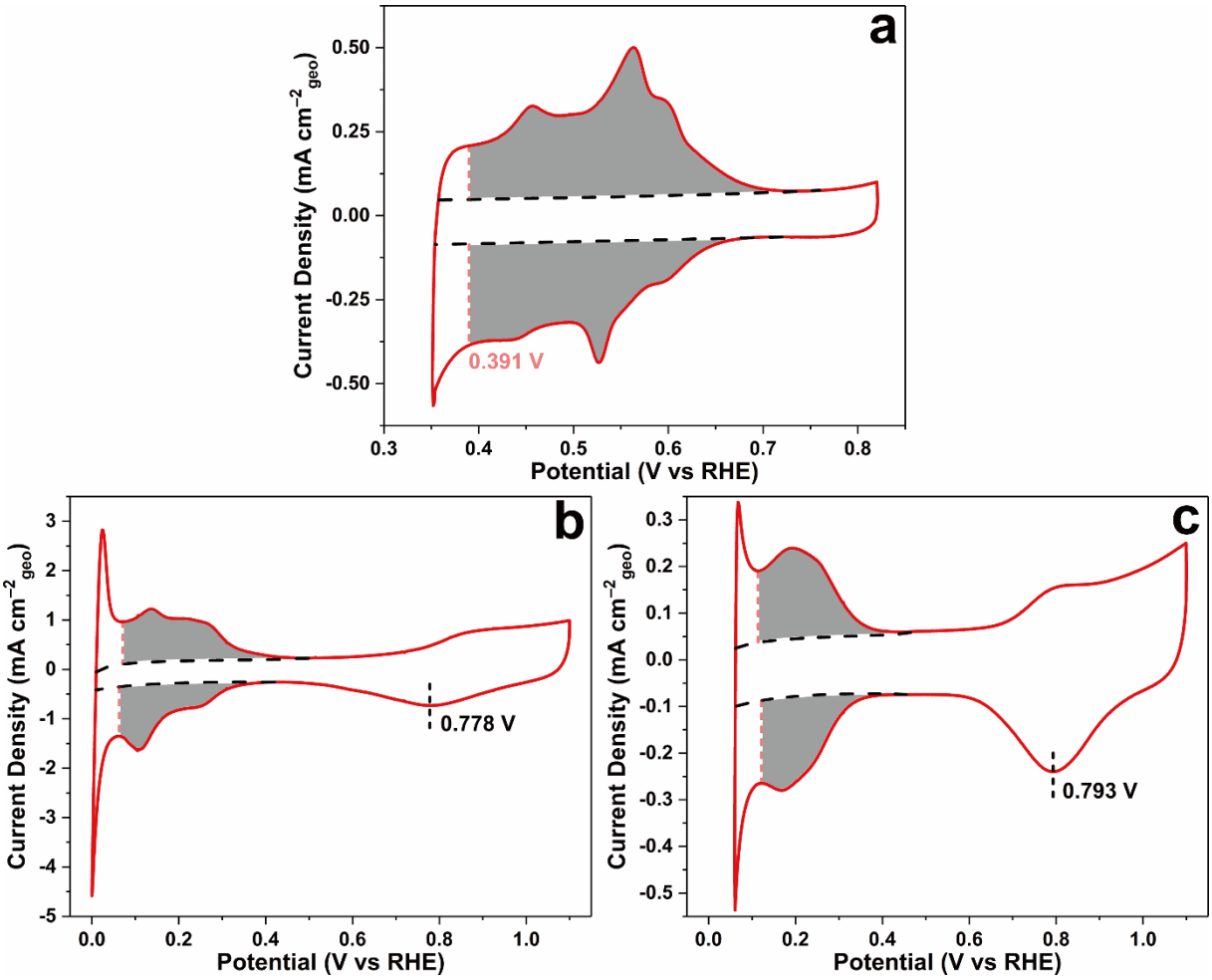

Fig. S2 (a) Representative CV for the Cu UPD on $^{CG}Cu_1Pd_1$ NSs/C-HT at 20 mV s^{-1}. Representative CVs for (b) the commercial Pt/C and (c) $^{CG}Cu_1Pd_1@Pt_{ML}$ NSs/C-HT in N_2-saturated 0.1 M $HClO_4$ solutions at 20 mV s^{-1}. The two black short dash lines represent the corresponding electric double layer charge-discharge currents caused by the supports. The shaded areas represent the associated Cu/H adsorption (lower parts) and desorption (upper parts) areas.

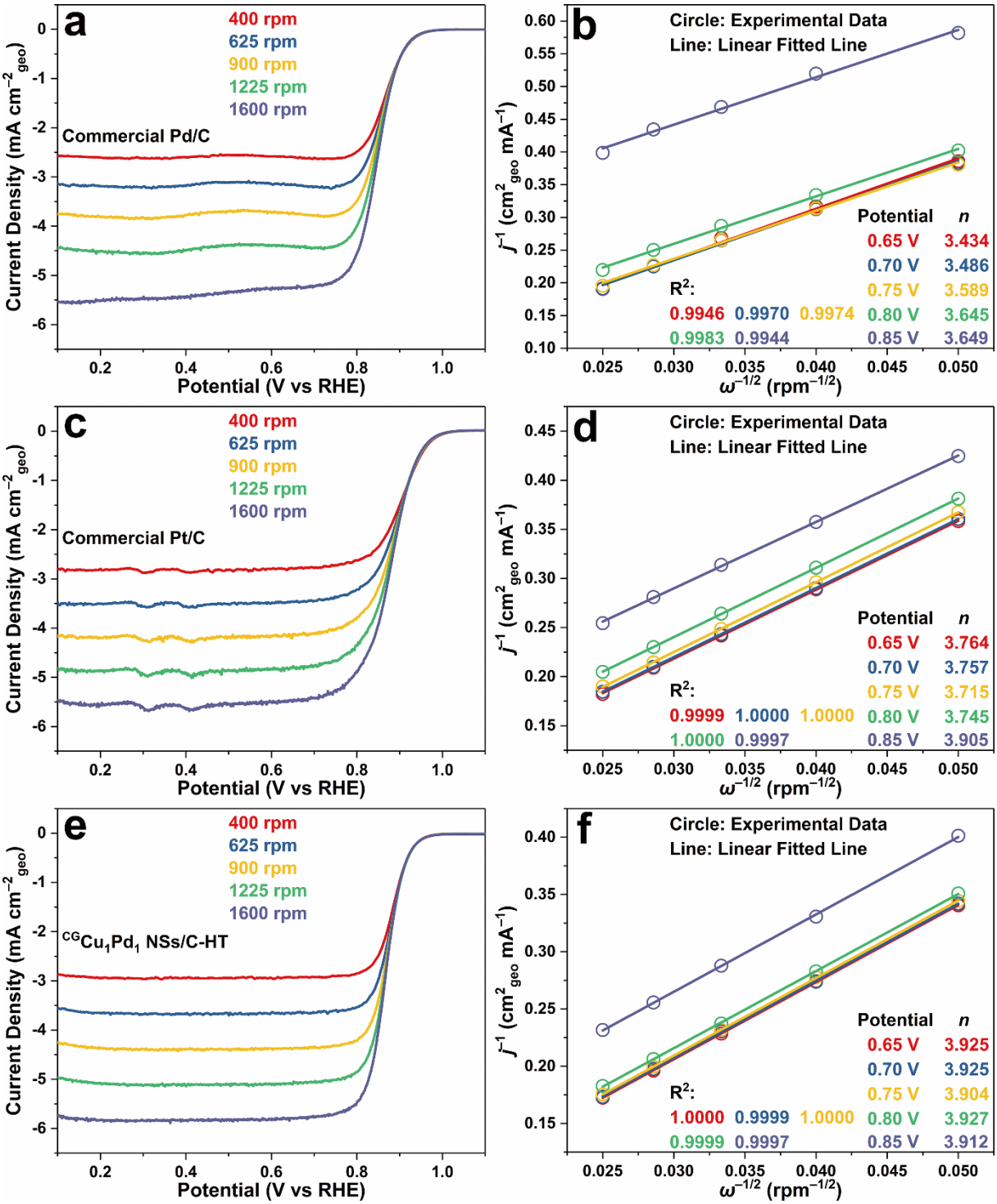

Fig. S3 Representative LSVs from 400 to 1600 rpm at 10 mV s^{-1} for (a) the commercial Pd/C, (c) Pt/C and (e) $^{CG}Cu_1Pd_1$ NSs/C-HT in O_2-saturated 0.1 M KOH solutions. (b, d and f) Associated K-L plots derived from (a, c and e).

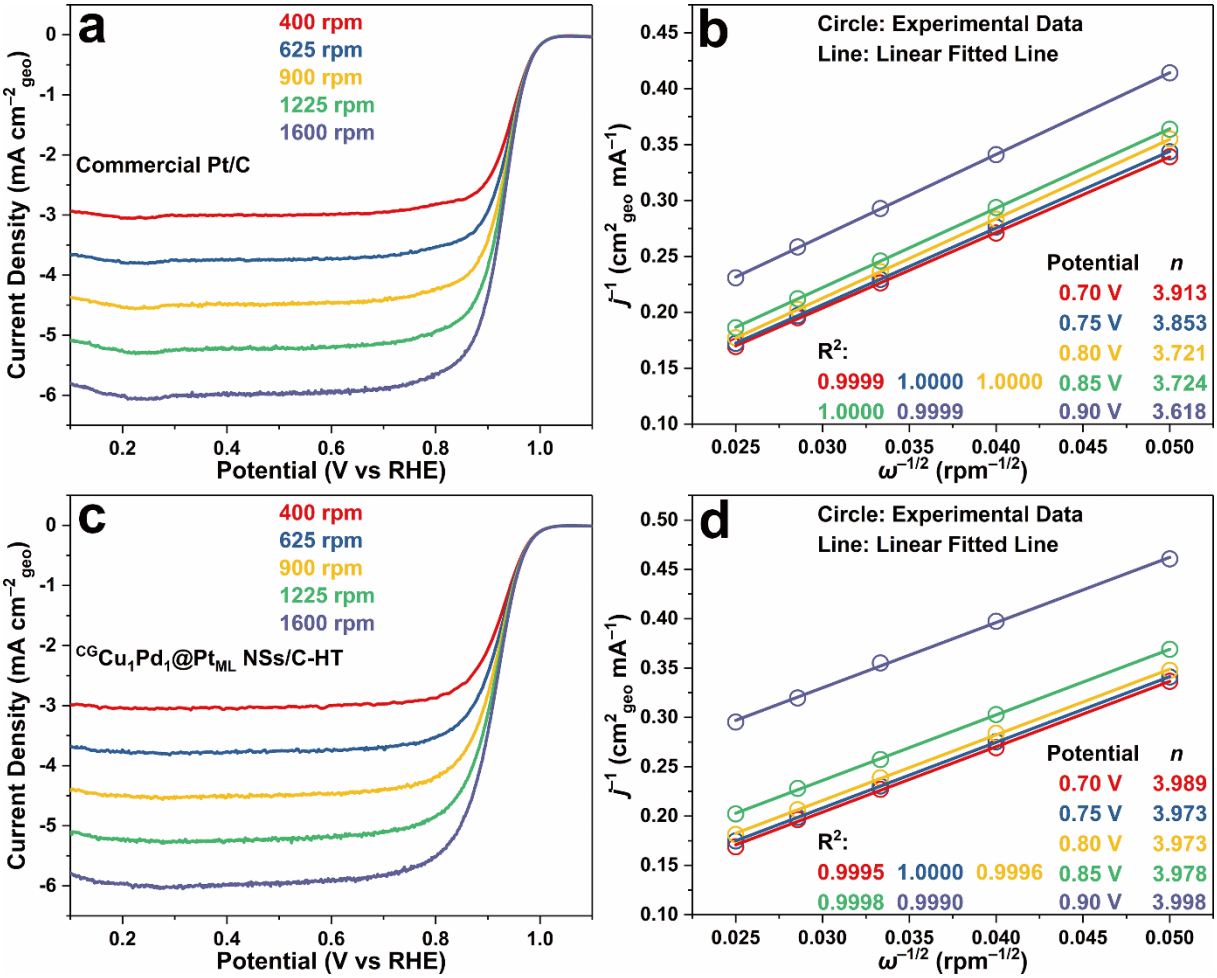

Fig. S4 Representative LSVs from 400 to 1600 rpm at 10 mV s^{-1} for (a) the commercial Pt/C and (c) $^{CG}Cu_1Pd_1@Pt_{ML}$ NSs/C-HT in O_2-saturated 0.1 M $HClO_4$ solutions. (b and d) Associated K-L plots derived from (a and c).

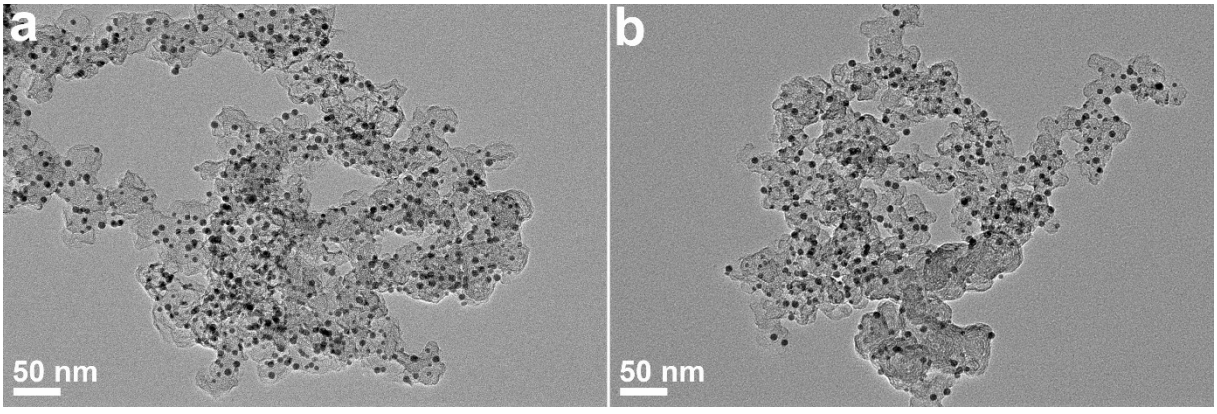

Fig. S5 Representative TEM images of (a) $^{CG}Cu_1Pd_1$ and (b) $^{CG}Cu_1Pd_1@Pt_{ML}$ NSs/C-HTs after the respective 20000 and 10000 cycles of the ADT.

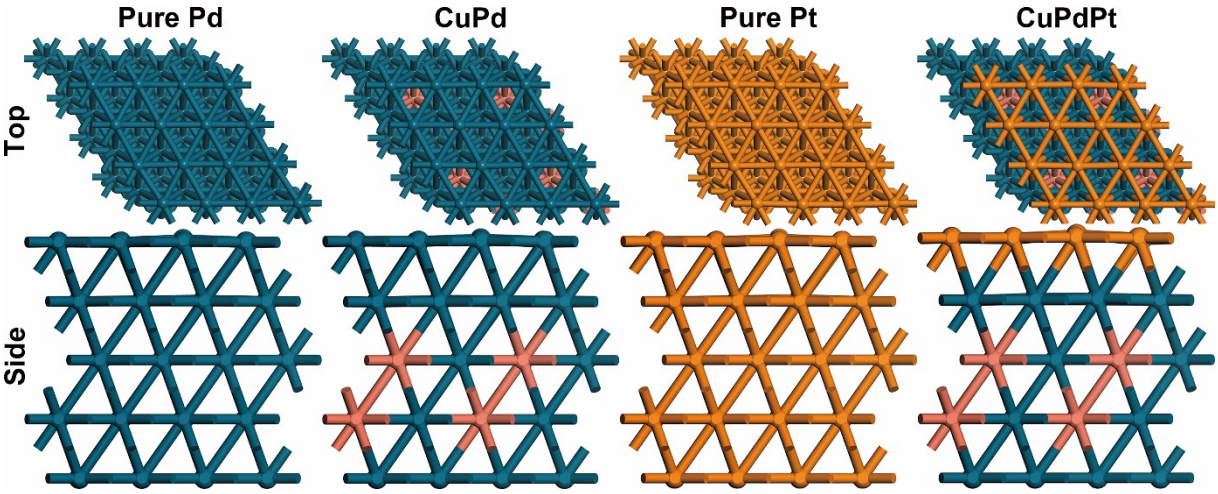

Fig. S6 Structure-optimized slabs for pure Pd, pure Pt, CuPd and CuPdPt. The sienna color represents Cu, while the navy color represents Pd, and dark orange, Pt.

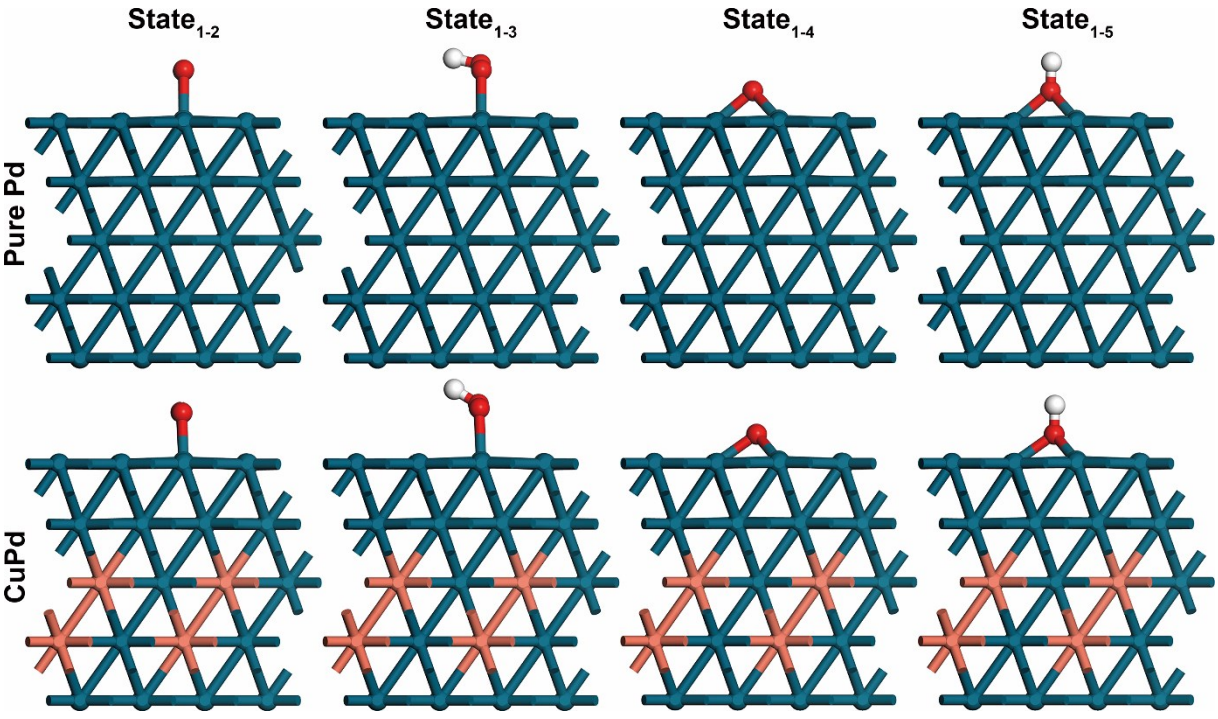

Fig. S7 Structure-optimized pure Pd and CuPd slabs adsorbed with the intermediates from different states, which are presented in side view, and the slabs in top view are previously shown in Fig. 9.

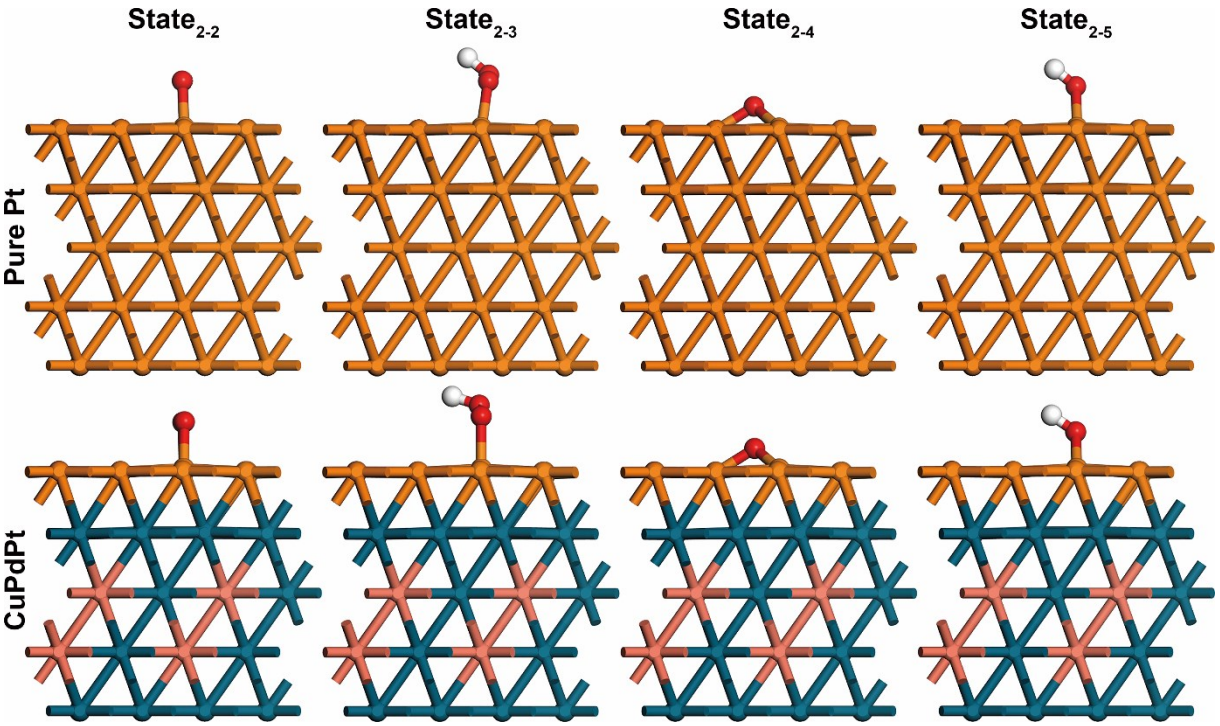

Fig. S8 Structure-optimized pure Pt and CuPdPt slabs adsorbed with the intermediates from different states, which are presented in side view, and the slabs in top view are previously shown in Fig. 10.

Table S1–S4

Table S1 Detailed alkaline ORR electrocatalytic properties of the commercial Pd/C, Pt/C, $^{CG}Cu_1Pd_1$ NSs/C and $^{CG}Cu_1Pd_1$ NSs/C-HT[a]

electrocatalyst	ECSA ($m^2\ g^{-1}_{Pd/Pt}$)	ASA ($mA\ cm^{-2}$)	MSA ($mA\ mg^{-1}_{Pd/Pt}$)	enhancement factor
commercial Pd/C	26.63_{Cu_UPD}	0.165	44	N/A
commercial Pt/C	59.62_{H}	0.149	89	N/A
$^{CG}Cu_1Pd_1$ NSs/C	76.88_{Cu_UPD}	0.680	523	$4.1_{ASA(Pd)}$ $4.6_{ASA(Pt)}$ $11.9_{MSA\text{-}Pd(Pd)}$ $5.9_{MSA\text{-}Pd(Pt)}$
$^{CG}Cu_1Pd_1$ NSs/C-HT	77.25_{Cu_UPD}	0.781	603	$4.7_{ASA(Pd)}$ $5.2_{ASA(Pt)}$ $13.7_{MSA\text{-}Pd(Pd)}$ $6.8_{MSA\text{-}Pd(Pt)}$

[a] The ECSAs of the commercial Pd/C and $^{CG}Cu_1Pd_1$ NSs/C are quoted from our previous work for comparison.[1] The Pd(Pt) means that the Pd-based ORR electrocatalytic activity of the electrocatalyst is compared to the associated commercial Pt/C, and so on.

Table S2 Detailed acidic ORR electrocatalytic properties of the commercial Pt/C and $^{CG}Cu_1Pd_1@Pt_{ML}$ NSs/C-HT

electrocatalyst	ECSA ($m^2\ g^{-1}$)	ASA ($mA\ cm^{-2}$)	MSA ($mA\ mg^{-1}$)	enhancement factor
commercial Pt/C	$59.62_{H\text{-}Pt}$	0.332	198_{Pt}	N/A
$^{CG}Cu_1Pd_1@Pt_{ML}$ NSs/C-HT	$82.70_{H\text{-}Pd}$ $236.36_{H\text{-}Pt}$	1.110	680_{NM} 2624_{Pt}	3.4_{ASA} $3.4_{MSA\text{-}NM}$ $13.3_{MSA\text{-}Pt}$

Table S3 A comprehensive literature survey for the ORR electrocatalytic activity (@0.9 V vs RHE) of the excellent non-Pt Pd-based electrocatalysts in alkaline media reported in the past 10 years

electrocatalyst	testing condition	MSA ($mA\ mg^{-1}$)	ASA ($mA\ cm^{-2}$)	enhancement factor	reference
$^{CG}Cu_1Pd_1$ NSs/C-HT	0.1 M KOH 10 mV s^{-1} 1600 rpm	603_{Pd}	0.78_{Cu_UPD}	$\sim13.7_{MSA\text{-}Pd(Pd)}$ $\sim6.8_{MSA\text{-}Pd(Pt)}$ $\sim4.7_{ASA(Pd)}$ $\sim5.2_{ASA(Pt)}$	This Study
dendritic PdBP alloy MSs	0.1 M KOH 10 mV s^{-1} 1600 rpm	1450_{Pd}	$2.45_{O/OH}$	$\sim5.0_{MSA\text{-}Pd(Pd)}$ $\sim2.9_{MSA\text{-}Pd(Pt)}$ $\sim2.5_{ASA(Pd)}$ $\sim2.0_{ASA(Pt)}$	*ACS Nano*, 2019, **13**, 12052–12061.[14]
v-Pd_2CoAg NCs	0.1 M KOH 10 mV s^{-1} 1600 rpm	660_{Pd} $\sim476_{NM}$	$\sim0.48_{O/OH}$	$5.0_{MSA\text{-}Pd(Pt)}$ $\sim3.6_{MSA\text{-}NM(Pt)}$ $\sim2.8_{ASA(Pt)}$	*Appl. Catal. B Environ.*, 2019, **241**, 424–429.[15]
Pd_4Sn WNWs/C	0.1 M KOH 10 mV s^{-1} 1600 rpm	650_{Pd}	1.51_{CO}	$16.3_{MSA\text{-}Pd(Pd)}$ $7.2_{MSA\text{-}Pd(Pt)}$ $18.8_{ASA(Pd)}$ $9.4_{ASA(Pt)}$	*Nano Lett.*, 2019, **19**, 6894–6903.[16]
IM-Pd_3Pb NNs	0.1 M KOH 10 mV s^{-1} 1600 rpm	610_{Pd}	$15.7_{O/OH}$	$\sim2.9_{MSA\text{-}Pd(Pt)}$ $\sim2.9_{ASA(Pt)}$	*J. Mater. Chem. A*, 2017, **5**, 23952–23959.[17]
Pd_3Pb/Pd NSs/C	0.1 M KOH 10 mV s^{-1} 1600 rpm	574_{Pd}	1.31_{CO}	$8.8_{MSA\text{-}Pd(Pd)}$ $6.5_{MSA\text{-}Pd(Pt)}$ $9.4_{ASA(Pd)}$ $9.8_{ASA(Pt)}$	*Nano Lett.*, 2019, **19**, 1336–1342.[18]
Pd_3Pb TPs/C	0.1 M KOH 10 mV s^{-1} 1600 rpm	560_{Pd}	1.76_{CO}	$8.4_{MSA\text{-}Pd(Pd)}$ $6.7_{MSA\text{-}Pd(Pt)}$ $12.0_{ASA(Pd)}$ $13.4_{ASA(Pt)}$	*Chem*, 2018, **4**, 359–371.[19]
Pd/MnO_2-CNT	0.1 M KOH 10 mV s^{-1} 1600 rpm	484_{Pd}	N/A	$24.2_{MSA\text{-}Pd(Pd)}$ $\sim37.2_{MSA\text{-}Pd(Pt)}$	*J. Mater. Chem. A*, 2018, **6**, 23366–23377.[20]
PdCuNi-AB-t/C	0.1 M NaOH 10 mV s^{-1} 1600 rpm	450_{Pd}	N/A	$2.4_{MSA\text{-}Pd(Pd)}$ $5.0_{MSA\text{-}Pd(Pt)}$	*Adv. Funct. Mater.*, 2018, **28**, 1707219.[21]
$Pd_{59}Cu_{30}Co_{11}$ dendritic nanoalloy	0.1 M KOH 10 mV s^{-1} 1600 rpm	380_{Pd}	0.90_{CO}	$\sim3.5_{MSA\text{-}Pd(Pt)}$ $\sim4.0_{ASA(Pt)}$	*Nat. Commun.*, 2018, **9**, 3702.[22]
Pd@NiO-0.3/C	0.1 M KOH 10 mV s^{-1} 1600 rpm	240_{Pd}	N/A	$\sim3.8_{MSA\text{-}Pd(Pd)}$ $2.2_{MSA\text{-}Pd(Pt)}$	*Nano Energy*, 2019, **58**, 234–243.[23]
icosahedral Pd_6Ni/C	0.1 M KOH 10 mV s^{-1} 1600 rpm	220_{Pd}	$0.66_{O/OH}$	$\sim3.7_{MSA\text{-}Pd(Pd)}$ $2.0_{MSA\text{-}Pd(Pt)}$ $\sim4.2_{ASA(Pd)}$ $\sim3.0_{ASA(Pt)}$	*Sci. Adv.*, 2018, **4**, eaap8817.[24]

$Pd/W_{18}O_{49}$	0.1 M KOH 10 mV s^{-1} 1600 rpm	216_{Pd}	$0.45_{O/OH}$	$10.0_{MSA\text{-}Pd(Pd)}$ $2.0_{MSA\text{-}Pd(Pt)}$ $\sim 22.5_{ASA(Pd)}$ $\sim 2.8_{ASA(Pt)}$	*J. Am. Chem. Soc.*, 2014, **136**, 11687–11697.[25]
ordered Pd_3Pb/C	0.1 M KOH 10 mV s^{-1} 1600 rpm	$\sim 169_{Pd}$	N/A	$\sim 4.4_{MSA\text{-}Pd(Pd)}$ $\sim 4.0_{MSA\text{-}Pd(Pt)}$	*Nano Lett.*, 2016, **16**, 2560–2566.[26]
PdCuCo NPs/C-375ºC	0.1 M NaOH 10 mV s^{-1} 1600 rpm	130_{Pd}	N/A	$3.3_{MSA\text{-}Pd(Pd)}$ $1.3_{MSA\text{-}Pd(Pt)}$	*Angew. Chem. Int. Ed.*, 2016, **55**, 9030–9035.[27]
AuPdCo/C intermetallic	0.1 M KOH 10 mV s^{-1} 1600 rpm	130_{NM}	N/A	$\sim 1.4_{MSA\text{-}NM(Pt)}$	*Nat. Commun.*, 2014, **5**, 5185.[28]
ordered Pd_3Fe/C	0.1 M KOH 10 mV s^{-1} 1600 rpm	$\sim 97_{Pd}$	N/A	$\sim 2.2_{MSA\text{-}Pd(Pd)}$ $\sim 1.3_{MSA\text{-}Pd(Pt)}$	*J. Am. Chem. Soc.*, 2015, **137**, 7278–7281.[29]
NP-PdCe	0.1 M KOH 10 mV s^{-1} 1600 rpm	$\sim 78_{Pd}$	$\sim 0.24_{O/OH}$	$\sim 5.2_{MSA\text{-}Pd(Pd)}$ $\sim 1.9_{ASA(Pd)}$	*J. Mater. Chem. A*, 2018, **6**, 23560–23568.[30]

Table S4 A comprehensive literature survey for the ORR electrocatalytic activity (@0.9 V vs RHE) of the excellent non-Pt-core@Pt-shell electrocatalysts in acidic media reported in the past 10 years

electrocatalyst	testing condition	MSA (mA mg^{-1})	ASA (mA cm^{-2})	enhancement factor	reference
$^{CG}Cu_1Pd_1@Pt_{ML}$ NSs/C-HT	0.1 M $HClO_4$ 10 mV s^{-1} 1600 rpm	2624_{Pt} 680_{NM}	1.11_{H}	$\sim13.3_{MSA\text{-}Pt}$ $\sim3.4_{MSA\text{-}NM}$ $\sim3.4_{ASA\text{-}H}$	This Study
$Pd_{20}Au$–Pt core-shell aerogel	0.1 M $HClO_4$ 10 mV s^{-1} 1600 rpm	5250_{Pt} 750_{NM}	2.53_{H}	$18.7_{MSA\text{-}Pt}$ $2.7_{MSA\text{-}NM}$ 4.1_{ASA}	*Angew. Chem. Int. Ed.*, 2018, **57**, 2963–2966.[31]
Pd@Pt–Ni/C	0.1 M $HClO_4$ 10 mV s^{-1} 1600 rpm	2500_{Pt} 1600_{NM}	2.70_{Cu_UPD}	$12.5_{MSA\text{-}Pt}$ $8.0_{MSA\text{-}NM}$ $\sim14.2_{ASA}$	*ACS Nano*, 2014, **8**, 10363–10371.[32]
$PtNi_{0.56}Pd_{1.42}$ NWs	0.1 M $HClO_4$ 10 mV s^{-1} 1600 rpm	1930_{Pt} 1090_{NM}	3.48_{CO}	$\sim12.1_{MSA\text{-}Pt}$ $\sim6.8_{MSA\text{-}NM}$ $\sim13.4_{ASA}$	*Adv. Mater.*, 2017, **29**, 1603774.[33]
ozone-treated Pt–Pd NW/C	0.1 M $HClO_4$ 10 mV s^{-1} 1600 rpm	1830_{Pt} 550_{NM}	0.77_{H}	$\sim9.6_{MSA\text{-}Pt}$ $\sim2.9_{MSA\text{-}NM}$ $\sim3.5_{ASA}$	*J. Am. Chem. Soc.*, 2011, **133**, 9783–9795.[6]
Pd@PtNi NWs/C	0.1 M $HClO_4$ 10 mV s^{-1} 1600 rpm	1750_{Pt} $\sim664_{NM}$	3.18_{H}	$\sim10.3_{MSA\text{-}Pt}$ $\sim3.9_{MSA\text{-}NM}$ $\sim11.8_{ASA}$	*Small*, 2019, **15**, 1900288.[34]
Pd@Pt concave decahedra	0.1 M $HClO_4$ 10 mV s^{-1} 1600 rpm	1600_{Pt} 474_{NM}	1.66_{H}	$5.0_{MSA\text{-}Pt}$ $\sim1.5_{MSA\text{-}NM}$ $\sim4.6_{ASA}$	*J. Am. Chem. Soc.*, 2015, **137**, 15036–15042.[35]
Pt_{ML}/Pd/C	0.1 M $HClO_4$ 10 mV s^{-1} 1600 rpm	1570_{Pt} 350_{NM}	$\sim0.69_{H}$	$\sim5.8_{MSA\text{-}Pt}$ $\sim1.3_{MSA\text{-}NM}$ $\sim1.9_{ASA}$	*J. Mater. Chem. A*, 2018, **6**, 20725–20736.[36]
Pt_{ML}AuNi-a/C	0.1 M $HClO_4$ 10 mV s^{-1} 1600 rpm	1520_{Pt} 340_{NM}	1.18_{H}	$\sim6.9_{MSA\text{-}Pt}$ $\sim1.5_{MSA\text{-}NM}$ $\sim4.7_{ASA}$	*Chem. Mater.*, 2016, **28**, 5274–5281.[37]
$Pd_{0.42}Ni_{0.58}$@Pt/C	0.1 M $HClO_4$ 10 mV s^{-1} 1600 rpm	1450_{Pt} 420_{NM}	0.61_{H}	$11.2_{MSA\text{-}Pt}$ $3.3_{MSA\text{-}NM}$ 2.8_{ASA}	*ACS Catal.*, 2017, **7**, 5420–5430.[2]
Pt~$Pd_{0.90}Ni_{0.10}$ nanowires	0.1 M $HClO_4$ 10 mV s^{-1} 1600 rpm	1440_{Pt}	0.62_{H}	$\sim10.3_{MSA\text{-}Pt}$ $\sim2.7_{ASA}$	*ACS Catal.*, 2014, **4**, 2544–2555.[38]
Pt_{ML}/IrNi/C	0.1 M $HClO_4$ 10 mV s^{-1} 1600 rpm	1400_{Pt} 780_{NM}	0.60_{H}	$\sim7.0_{MSA\text{-}Pt}$ $\sim3.9_{MSA\text{-}NM}$ 2.5_{ASA}	*Energy Environ. Sci.*, 2012, **5**, 5297–5304.[39]
fresh NPG–Pd–Pt	0.1 M $HClO_4$ 10 mV s^{-1} 1600 rpm	$\sim1130_{Pt}$ $\sim85_{NM}$	0.58_{H}	$\sim11.9_{MSA\text{-}Pt}$ $\sim0.9_{MSA\text{-}NM}$ $\sim4.2_{ASA}$	*Nat. Energy*, 2017, **2**, 17111.[40]
$Ti_{0.9}Cu_{0.1}$N@Pt/N CNTs	0.1 M $HClO_4$ 10 mV s^{-1} 1600 rpm	1060_{Pt}	0.69_{H}	$5.0_{MSA\text{-}Pt}$ 3.3_{ASA}	*ACS Catal.*, 2017, **7**, 3810–3817.[41]

$Pd_1Ru_1Ni_2$@Pt/C	0.1 M $HClO_4$ 10 mV s^{-1} 1600 rpm	1060_{Pt} $\sim 269_{NM}$	0.57_H	$\sim 5.1_{MSA\text{-}Pt}$ $\sim 1.3_{MSA\text{-}NM}$ $\sim 3.2_{ASA}$	*J. Mater. Chem. A*, 2016, **4**, 847–855.[42]
Pd@Pt octahedra	0.1 M $HClO_4$ 10 mV s^{-1} 1600 rpm	1050_{Pt} 346_{NM}	1.51_H	$\sim 3.3_{MSA\text{-}Pt}$ $\sim 1.1_{MSA\text{-}NM}$ $\sim 4.2_{ASA}$	*J. Am. Chem. Soc.*, 2016, **138**, 12263–12270.[43]
PtNiN/C	0.1 M $HClO_4$ 10 mV s^{-1} 1600 rpm	860_{Pt}	1.65_H	$4.3_{MSA\text{-}Pt}$ $\sim 6.9_{ASA}$	*Nano Lett.*, 2012, **12**, 6266–6271.[44]
PtFeN/C	0.1 M $HClO_4$ 10 mV s^{-1} 1600 rpm	820_{Pt}	1.37_H	$4.1_{MSA\text{-}Pt}$ $\sim 5.7_{ASA}$	*Nano Energy*, 2015, **13**, 442–449.[45]
TiNiN@Pt	0.1 M $HClO_4$ 10 mV s^{-1} 1600 rpm	830_{Pt}	0.49_H	$\sim 4.0_{MSA\text{-}Pt}$ $\sim 2.0_{ASA}$	*J. Am. Chem. Soc.*, 2016, **138**, 1575–1583.[46]
Pd@Pt–Ni/C	0.1 M $HClO_4$ 10 mV s^{-1} 1600 rpm	790_{Pt} 480_{NM}	$\sim 0.44_H$	$\sim 4.9_{MSA\text{-}Pt}$ $3.0_{MSA\text{-}NM}$ $\sim 1.8_{ASA}$	*J. Am. Chem. Soc.*, 2015, **137**, 2804–2807.[47]
Pd@Pt/C	0.1 M $HClO_4$ 10 mV s^{-1} 1600 rpm	780_{Pt} 230_{NM}	0.55_H	$3.9_{MSA\text{-}Pt}$ $\sim 1.2_{MSA\text{-}NM}$ $\sim 2.3_{ASA}$	*ACS Catal.*, 2016, **6**, 3428–3432.[48]
Pd@Pt_{1L}/C	0.1 M $HClO_4$ 10 mV s^{-1} 1600 rpm	750_{Pt} $\sim 285_{NM}$	1.01_H	$\sim 2.7_{MSA\text{-}Pt}$ $\sim 1.0_{MSA\text{-}NM}$ $\sim 2.9_{ASA}$	*Chem. Mater.*, 2019, **31**, 1370–1380.[49]
Pt_{ML}/Pd_{ML}/Ir_2ReML_1/C	0.1 M $HClO_4$ 10 mV s^{-1} 1600 rpm	600_{Pt} 180_{NM}	$\sim 0.27_H$	$\sim 3.5_{MSA\text{-}Pt}$ $\sim 1.1_{MSA\text{-}NM}$ $\sim 1.1_{ASA}$	*ACS Catal.*, 2012, **2**, 817–824.[50]
5.8 nm Ni/FePt	0.1 M $HClO_4$ 10 mV s^{-1} 1600 rpm	490_{Pt}	1.95_H	$\sim 5.3_{MSA\text{-}Pt}$ $\sim 5.7_{ASA}$	*J. Am. Chem. Soc.*, 2014, **136**, 15921–15924.[51]
Pd@$Pt_{2–3L}$/C	0.1 M $HClO_4$ 10 mV s^{-1} 1600 rpm	490_{Pt} $\sim 149_{NM}$	0.91_H	$\sim 5.5_{MSA\text{-}Pt}$ $\sim 1.7_{MSA\text{-}NM}$ $\sim 5.4_{ASA}$	*ACS Nano*, 2015, **9**, 2635–2647.[52]
Au@Ni_6Pt_2/C	0.1 M $HClO_4$ 10 mV s^{-1} 1600 rpm	445_{Pt} $\sim 300_{NM}$	$\sim 0.57_H$	$\sim 2.3_{MSA\text{-}Pt}$ $\sim 1.6_{MSA\text{-}NM}$ $\sim 2.0_{ASA}$	*ACS Catal.*, 2016, **6**, 1680–1690.[53]
PdCu A1@PtCu/C	0.1 M $HClO_4$ 10 mV s^{-1} 1600 rpm	$\sim 100_{Pt}$ $\sim 51_{NM}$	0.23_H	$\sim 2.0_{MSA\text{-}Pt}$ $\sim 1.0_{MSA\text{-}NM}$ $\sim 3.1_{ASA}$	*ACS Nano*, 2019, **13**, 4008–4017.[54]

Supplementary references

1 L. Luo, C. Fu, F. Yang, X. Li, F. Jiang, Y. Guo, F. Zhu, L. Yang, S. Shen and J. Zhang, *ACS Catal.*, 2020, **10**, 1171–1184.
2 L. Luo, F. Zhu, R. Tian, L. Li, S. Shen, X. Yan and J. Zhang, *ACS Catal.*, 2017, **7**, 5420–5430.
3 L. Luo, C. Fu, X. Yan, S. Shen, F. Yang, Y. Guo, F. Zhu, L. Yang and J. Zhang, *ACS Appl. Mater. Interfaces*, 2020, **12**, 25961–25971.
4 J. Zhang, Y. Mo, M. B. Vukmirovic, R. Klie, K. Sasaki and R. R. Adzic, *J. Phys. Chem. B*, 2004, **108**, 10955–10964.
5 J. Zhang, F. H. Lima, M. H. Shao, K. Sasaki, J. X. Wang, J. Hanson and R. R. Adzic, *J. Phys. Chem. B*, 2005, **109**, 22701–22704.
6 C. Koenigsmann, A. C. Santulli, K. Gong, M. B. Vukmirovic, W.-p. Zhou, E. Sutter, S. S. Wong and R. R. Adzic, *J. Am. Chem. Soc.*, 2011, **133**, 9783–9795.
7 G. Kresse and J. Hafner, *Phys. Rev. B*, 1993, **47**, 558–561.
8 G. Kresse and J. Hafner, *Phys. Rev. B*, 1994, **49**, 14251–14269.
9 G. Kresse and J. Furthmüller, *Comput. Mater. Sci.*, 1996, **6**, 15–50.
10 G. Kresse and J. Furthmuller, *Phys. Rev. B*, 1996, **54**, 11169–11186.
11 G. Kresse and D. Joubert, *Phys. Rev. B*, 1999, **59**, 1758–1775.
12 P. E. Blochl, *Phys. Rev. B*, 1994, **50**, 17953–17979.
13 J. K. Nørskov, J. Rossmeisl, A. Logadottir, L. Lindqvist, J. R. Kitchin, T. Bligaard and H. Jónsson, *J. Phys. Chem. B*, 2004, **108**, 17886–17892.
14 H. Lv, D. Xu, L. Sun, J. Henzie, S. L. Suib, Y. Yamauchi and B. Liu, *ACS Nano*, 2019, **13**, 12052–12061.
15 S. Liu, H. Zhang, X. Mu and C. Chen, *Appl. Catal. B Environ.*, 2019, **241**, 424–429.
16 Y. Zhang, B. Huang, Q. Shao, Y. Feng, L. Xiong, Y. Peng and X. Huang, *Nano Lett.*, 2019, **19**, 6894–6903.
17 Q. Shi, C. Zhu, C. Bi, H. Xia, M. H. Engelhard, D. Du and Y. Lin, *J. Mater. Chem. A*, 2017, **5**, 23952–23959.
18 C. Tang, N. Zhang, Y. Ji, Q. Shao, Y. Li, X. Xiao and X. Huang, *Nano Lett.*, 2019, **19**, 1336–1342.
19 L. Bu, Q. Shao, Y. Pi, J. Yao, M. Luo, J. Lang, S. Hwang, H. Xin, B. Huang, J. Guo, D. Su, S. Guo and X. Huang, *Chem*, 2018, **4**, 359–371.
20 W. Xiang, Y. Zhao, Z. Jiang, X. Li, H. Zhang, Y. Sun, Z. Ning, F. Du, P. Gao, J. Qian, K. Kato, M. Yamauchi and Y. Sun, *J. Mater. Chem. A*, 2018, **6**, 23366–23377.
21 H. Wang, W. Luo, L. Zhu, Z. Zhao, B. E, W. Tu, X. Ke, M. Sui, C. Chen, Q. Chen, Y. Li and Y. Huang, *Adv. Funct. Mater.*, 2018, **28**, 1707219.
22 C. Li, Q. Yuan, B. Ni, T. He, S. Zhang, Y. Long, L. Gu and X. Wang, *Nat. Commun.*, 2018, **9**, 3702.
23 Y. Feng, C. Yang, W. Fang, B. Huang, Q. Shao and X. Huang, *Nano Energy*, 2019, **58**, 234–243.
24 Y. Feng, Q. Shao, Y. Ji, X. Cui, Y. Li, X. Zhu and X. Huang, *Sci. Adv.*, 2018, **4**, eaap8817.
25 Y. Lu, Y. Jiang, X. Gao, X. Wang and W. Chen, *J. Am. Chem. Soc.*, 2014, **136**, 11687–11697.
26 Z. Cui, H. Chen, M. Zhao and F. J. DiSalvo, *Nano Lett.*, 2016, **16**, 2560–2566.
27 K. Jiang, P. Wang, S. Guo, X. Zhang, X. Shen, G. Lu, D. Su and X. Huang, *Angew. Chem. Int. Ed.*, 2016, **55**, 9030–9035.
28 K. A. Kuttiyiel, K. Sasaki, D. Su, L. Wu, Y. Zhu and R. R. Adzic, *Nat. Commun.*, 2014, **5**, 5185.
29 Z. Cui, L. Li, A. Manthiram and J. B. Goodenough, *J. Am. Chem. Soc.*, 2015, **137**, 7278–7281.
30 J. Chen, Y. Li, N. Lu, C. Tian, Z. Han, L. Zhang, Y. Fang, B. Qian, X. Jiang and R. Cui, *J. Mater. Chem. A*, 2018, **6**, 23560–23568.
31 B. Cai, R. Hubner, K. Sasaki, Y. Zhang, D. Su, C. Ziegler, M. B. Vukmirovic, B. Rellinghaus, R. R. Adzic and A. Eychmuller, *Angew. Chem. Int. Ed.*, 2018, **57**, 2963–2966.
32 S.-I. Choi, M. Shao, N. Lu, A. Ruditskiy, H.-C. Peng, J. Park, S. Guerrero, J. Wang, M. J. Kim and Y. Xia, *ACS Nano*, 2014, **8**, 10363–10371.
33 N. Zhang, Y. Feng, X. Zhu, S. Guo, J. Guo and X. Huang, *Adv. Mater.*, 2017, **29**, 1603774.
34 Y. Zhao, L. Tao, W. Dang, L. Wang, M. Xia, B. Wang, M. Liu, F. Gao, J. Zhang and Y. Zhao, *Small*, 2019, **15**, e1900288.
35 X. Wang, M. Vara, M. Luo, H. Huang, A. Ruditskiy, J. Park, S. Bao, J. Liu, J. Howe, M. Chi, Z. Xie and Y. Xia, *J. Am. Chem. Soc.*, 2015, **137**, 15036–15042.
36 G. Chen, K. A. Kuttiyiel, M. Li, D. Su, L. Du, C. Du, Y. Gao, W. Fei, G. Yin, K. Sasaki and R. R. Adzic, *J. Mater. Chem. A*, 2018, **6**, 20725–20736.
37 G. Chen, K. A. Kuttiyiel, D. Su, M. Li, C.-H. Wang, D. Buceta, C. Du, Y. Gao, G. Yin, K. Sasaki, M. B. Vukmirovic and R. R. Adzic, *Chem. Mater.*, 2016, **28**, 5274–5281.
38 H. Liu, C. Koenigsmann, R. R. Adzic and S. S. Wong, *ACS Catal.*, 2014, **4**, 2544–2555.
39 K. A. Kuttiyiel, K. Sasaki, Y. Choi, D. Su, P. Liu and R. R. Adzic, *Energy Environ. Sci.*, 2012, **5**, 5297–5304.
40 J. Li, H.-M. Yin, X.-B. Li, E. Okunishi, Y.-L. Shen, J. He, Z.-K. Tang, W.-X. Wang, E. Yücelen, C. Li, Y. Gong, L. Gu, S. Miao, L.-M. Liu, J. Luo and Y. Ding, *Nat. Energy*, 2017, **2**, 17111.
41 X. Tian, H. Tang, J. Luo, H. Nan, T. Shu, L. Du, J. Zeng, S. Liao and R. R. Adzic, *ACS Catal.*, 2017, **7**, 3810–3817.
42 H. Nan, X. Tian, J. Luo, D. Dang, R. Chen, L. Liu, X. Li, J. Zeng and S. Liao, *J. Mater. Chem. A*, 2016, **4**, 847–855.
43 M. Zhou, H. Wang, M. Vara, Z. D. Hood, M. Luo, T.-H. Yang, S. Bao, M. Chi, P. Xiao, Y. Zhang and Y. Xia, *J. Am. Chem. Soc.*, 2016, **138**, 12263–12270.
44 K. A. Kuttiyiel, K. Sasaki, Y. Choi, D. Su, P. Liu and R. R. Adzic, *Nano Lett.*, 2012, **12**, 6266–6271.
45 K. A. Kuttiyiel, Y. Choi, S.-M. Hwang, G.-G. Park, T.-H. Yang, D. Su, K. Sasaki, P. Liu and R. R. Adzic, *Nano Energy*, 2015, **13**, 442–449.
46 X. Tian, J. Luo, H. Nan, H. Zou, R. Chen, T. Shu, X. Li, Y. Li, H. Song, S. Liao and R. R. Adzic, *J. Am. Chem. Soc.*, 2016, **138**, 1575–1583.
47 X. Zhao, S. Chen, Z. Fang, J. Ding, W. Sang, Y. Wang, J. Zhao, Z. Peng and J. Zeng, *J. Am. Chem. Soc.*, 2015, **137**, 2804–2807.
48 L. Zhang, S. Zhu, Q. Chang, D. Su, J. Yue, Z. Du and M. Shao, *ACS Catal.*, 2016, **6**, 3428–3432.
49 M. Zhou, H. Wang, A. O. Elnabawy, Z. D. Hood, M. Chi, P. Xiao, Y. Zhang, M. Mavrikakis and Y. Xia, *Chem. Mater.*, 2019, **31**, 1370–1380.
50 H. I. Karan, K. Sasaki, K. Kuttiyiel, C. A. Farberow, M. Mavrikakis and R. R. Adzic, *ACS Catal.*, 2012, **2**, 817–824.
51 S. Zhang, Y. Hao, D. Su, V. V. Doan-Nguyen, Y. Wu, J. Li, S. Sun and C. B. Murray, *J. Am. Chem. Soc.*, 2014, **136**, 15921–15924.
52 J. Park, L. Zhang, S.-I. Choi, L. T. Roling, N. Lu, J. A. Herron, S. Xie, J. Wang, M. J. Kim, M. Mavrikakis and Y. Xia, *ACS Nano*, 2015, **9**, 2635–2647.
53 L.-L. Shen, G.-R. Zhang, S. Miao, J. Liu and B.-Q. Xu, *ACS Catal.*, 2016, **6**, 1680–1690.
54 J. T. L. Gamler, A. Leonardi, H. M. Ashberry, N. N. Daanen, Y. Losovyj, R. R. Unocic, M. Engel and S. E. Skrabalak, *ACS Nano*, 2019, **13**, 4008–4017.